Journal of Bio- and Tribo-Corrosion (2024) 10:8
https://doi.org/10.1007/s40735-023-00812-2

Electrochemical and Tribological Performance of Ti–Al with xNb Addition Synthesized via Laser In situ Alloying

L. R. Kanyane[1] · S. A. Raji[1] · M. Tlotleng[2,3]

Received: 8 September 2023 / Revised: 23 November 2023 / Accepted: 30 November 2023 / Published online: 2 January 2024

Abstract
Additive manufacturing is a growing technique of producing 3D parts directly using metal powders or wires melted with a high-powered intensity beam or laser. It is still a challenging process as to how laser processing parameters such as gas flow rate and powder flow rate can profitably be adopted to significantly produce Ti–Al-based materials from elemental powders to synthesize alloys that are defect-free and have good mechanical properties. The density of titanium aluminide (Ti–Al) intermetallic alloys makes it gain lots of interests due to its potential ability to substitute nickel-based superalloys in gas turbine engines. This work aims to investigate the effects of Niobium (Nb) additions on Ti–Al–xNb ternary alloys created via the use of 3D printing technology, specifically looking at microstructural evolution, microhardness, electrochemical behavior, and tribological properties. Ti–Al–Nb alloy was synthesized at scan speed of 26 in/min and laser power of 450 W. The structural morphology of the alloys produced was investigated using scanning electron microscopy equipped with energy dispersive spectroscopy and the electrochemical studies of the in situ alloyed Ti–Al–*x*Nb were studied using potentiodynamic techniques. Using an Emco microhardness tester, the microhardness characteristics of the produced TiAl–xNb alloys were examined. From the results obtained, it was observed that the microstructure showed not much substantial cracking or crack initiation. The micrographs are evident of refined microstructure associated to increase in Nb feed rate with α-Ti_3Al, γ-TiAl and precipitates of β-TiAl phases as the distinctively identified in the microstructure. The highest recorded microhardness value of 679.1 $HV_{0.5}$ was achieved at Nb feed of 0.5 rpm and gas carrier of 2 L/min. The fabricated Ti–Al–Nb alloys showed good corrosion resistance behavior in HCl and appreciable wear characteristics with coefficient of friction of 0.412, 0.401, and 0.414 μ at B1, B3, and B5, respectively.

Keywords In situ alloying · Additive manufacturing (AM) · Electrochemical behavior · Tribology

1 Introduction

Over the past three decades, alloys based on titanium aluminide (Ti–Al) have attracted a lot of attention because of their intriguing qualities. Several industries that include the aerospace, marine, automobile, and chemical industries consider this class of intermetallic alloys to be outstanding given their light-weightiness and stability under high temperature and to this end they are considered future best material to replace Nickel (Ni)-based super alloys [1, 2]. There are several stable phases of this alloy, but only one; the gamma phase alloy is considered to have appreciable engineering applications. The binary Ti–Al phase diagrams indicate that the gamma phase alloy is chemically balanced in the mixing of elemental powders which are titanium-Ti and aluminum-Al [1–5].

The binary Ti–Al alloy, consisting of 52Ti and 48Al (at.%), lacks ductility at room temperature (RT). This room temperature property makes them difficult to manufacture into finished products, and therefore has limited their industrialization programs. In addition, they are known to have poor wear and corrosion resistance to low microhardness

✉ L. R. Kanyane
Lrkanyane@gmail.com

[1] Department of Chemical, Metallurgical and Materials Engineering, Tshwane University of Technology, P.M.B. X680, Pretoria, South Africa

[2] Laser Enabled Manufacturing Research Group, Photonic Centre, Council of Scientific and Industrial Research (CSIR), Pretoria 0001, South Africa

[3] Material Science Innovation and Modelling Research Group, North-West University, Mahikeng Campus, Mmabatho, South Africa

property. Prosperous research on improving the ductility, mechanical and electrochemical behavior of this binary Ti–Al alloys has been achieved through the utilization of adding micro-alloying metallic (X) elements which are able to stabilize either the alpha or gamma phase or both giving rise to a super-stable alloy with improved machinability and engineering properties.The ternary Ti–Al–X alloys that have been investigated include and are not limited to TiAl–Mo [1], TiAl–Nb [2], TiAl–Cr [3], TiAl–Si [4], and others.

The development-adapted for the production of the third and fourth generation gamma Ti–Al alloys has brought their advance use into the commercial concepts in the aero-structures and automobile industries. Generally speaking, these two generation alloys are called TNB and TNM^{+} alloys, respectively. Their most texture-free microstructure is made possible by their disordered body-centered cubic (bcc; A2 structure) face and β-TiAl phase solidification, as reported in [4]. Heat treatment procedures are used to cure the microstructural features that are detrimental in order to improve the operating temperatures and performance properties [6–10]. A fully lamellar microstructure is produced by reducing the β_o-TiAl phase, which has an ordered bcc (B2 structure), and the globular γ-TiAl grains, which have an ordered face-centered tetragonal (FCT, L10 structure) [4]. Heat treatment (HT) above the intended service temperature can be used to accomplish this within the α-Ti (Al) single-phase field region (disordered hexagonal; A3 structure) [11]. According to Refs. [12, 13], the selected parameters affect the evolving α_2/γ lamellae colonies' grain size and lamellar spacing. Although the FL microstructure is known to have a better mix of strength and other characteristics, it is not very ductile [4].

When the base metal was preheated, there were fewer cracks visible on the coatings than when the substrate was not heated beforehand. The process's high cooling rate led to a maximum microhardness of 430 HV, which is greater than the microhardness of cast TiAl alloy. The stable and compact oxidation film of TiAl-based alloys is responsible for their good corrosion resistance properties [14]. The oxide layer that shields the alloy from deterioration can form on the surface quickly and on its own. In sulfuric acid, Bodunrin and Chown [15] looked into the anodic dissolution of Ti-based alloys. The titanium alloy, according to the authors, dissolves as Ti3 + directly and forms a thin layer of TiH2 on its surface in place of soluble oxide. Consequently, the TiH_2 film dissolves in the active dissolution region in accordance with the reaction $TiH_2=Ti^{3+}+_2H^{+}+5e^{-}$. As a result, the metal reactivates on its own because the passive oxide film dissolves, hastening the titanium alloy's corrosion.

In general, given that these intermetallics are crack-sensitive, casting [5, 6] as a preferred manufacturing tool had to be advanced by incorporating hot isostatic pressing which heals cracks and increases structural density. However, with the new developments of additive manufacturing, which give rise to massive production, Ti–Al components are now produced using machines such as electron beam melting (EBM), while the Laser Engineered Net-Shaping (LENS) is preferred for studies that includes alloy developments [2] in addition to its being a bulk production manufacturing tool [16–19]. In this study the LENS was used to produce TNB-Ti–Al alloys that contained Nb [Ti–Al–Nb]. During the synthesis, the effects of Nb, as a micro-alloying element, was elucidate and produced sample alloys were studied for microstructure, hardness, corrosion, and tribology.

2 Materials and Methods

2.1 Materials

In this work, pure elemental powders of Ti, Al, and Nb were employed as feedstocks. Powders of Ti and Al had a spherical shape and ranged in particle size distribution from 45 to 90 µm. Weartech, South Africa, supplied the irregularly shaped Nb, while TLS Technik, Germany, supplied the powders. Following receipt, powders were deposited onto $140 \times 140 \times 7$ mm^3 Ti6Al4V substrates.

2.2 Methods

2.2.1 Laser Metal Deposition

The grade 5 titanium alloy Ti6Al4V base plate was utilized as a substrate for the Ti–Al–xNb alloys, which were fabricated using the LENS® 850-R system at the Photonic Centre Council of Scientific and Industrial Research (PC-CSIR) equipped with a computer integrated 1 KW IPG fiber laser. The base plates were cleaned with acetone and sandblasted before deposition. The depositing head of the LENS machine, which is managed by Optomec software control, version 3.1.6 (Optomec, Albuquerque, NM, USA), is connected to the laser fiber that was used. The created Ti–Al–xNb ternary alloys were created using an in situ laser alloying technique. The ability of the Optomec software to automatically control the laser beam, powder hoppers, and deposition head made this possible. The experimental procedure complements the efforts of Tlotleng and Pityana [2].

In order to develop the Ti–Al–xNb via laser in situ alloying, Table 1 shows the sample codes of the laser developed alloys along with their Nb feed rate. The developed alloys were fabricated at a scan speed of 26 inches per minute using a 450 W laser. Ti and Al had feed rates of 2 rpm and 1.4 rpm, respectively, which corresponded to powder feed rates of 2.21 g/min and 0.48 g/min. Table 1 shows that the center purge gas flow rate was 25 L/min, and that the gas

Table 1 Process parameters used to fabricate Ti–Al–Nb alloys

Sample ID	Nb feed rate (rpm)	Nb federate (g/min)	Nb weight (at. %)
B1	0.1	0.039	6
B3	0.3	0.048	12
B5	0.5	0.057	14

carriers for Ti, Al, and Nb were maintained at 4.1 L/min, 2.4 L/min, and 2 L/min, respectively.

2.2.2 Heat Treatment

In an environment rich in argon, heat treatment was carried out in a muffle furnace (Kejia Furnace, China). The temperature of the samples was raised to 1350 °C. Before furnace cooling (FC), the temperature was ramped up at a rate of 20 °C per minute and maintained there for two hours.

2.2.3 Sample Preparation and Characterization

The developed cube samples were divided into sections and set in a resin composed of epoxy. To assess the microstructural features of the mounted samples, they were first polished to a mirror finish and then ground and etched using Kroll's reagent solution. This process was carried out using a scanning electron microscope outfitted with an electron diffraction spectrometer (SEM/EDS) made by Joel (JSM-6010Plus/LAM, Peabody, MA, USA). The phases contained in the ternary alloys were determined using a PaNalytical Empyrean X-ray diffractometry (XRD) machine (PANalytical Empyrean model, Malvern Panalytical Ltd., Royston, UK).

2.2.4 Microhardness

The developed Ti–Al–xNb alloys were subjected to Vickers microhardness (HVN) measurements using a Zwick/Roell Indentec (ZHVμ) microhardness tester machine (Zwick Roell AG, Ulm, Germany). 500 gf of indentation load and a 15-s dwell time were the parameters set. For every sample, ten indentations were tested; the average values are given. The following Eq. 1 can be used to calculate the variables related to the material's microhardness.

$$HVN = \frac{2F\mathrm{Sin}(136°)}{d^2} = 1.854\frac{F}{d^2} \quad (1)$$

2.2.5 Nano-indentation

The behavior of the manufactured alloys under nano-indentation was investigated using the Anton-Paar TTX-NHT3 nano-indentation tester. The apparatus has a 20 nm-radius Berkovich indenting tip. A 4 by 4 matrix array, or 16 indents, was recorded during the indentation process. A loading force of 200 mN was applied, and a holding and unloading duration of 20 s was observed. The Oliver and Pharr method was used to analyze the load–displacement curves in order to find material properties like stiffness, indentation hardness, and young's modulus.

2.2.6 Wear Test

Following the ASTM G99-95 standard, the tribological behavior of the synthesized Ti–Al–xNb was examined using Anton Paar tribology testing apparatus (Anton Paar, TRB3). In the test, a stainless steel pin-on-disc was utilized. A sliding distance of 3 mm was used with an applied load of 15N. For 900 s, the dry tribological test was conducted. The test yielded data on wear rate and coefficient of friction (CoF).

2.2.7 Corrosion Test

The Autolab Potentiostat was used to measure the linear polarization of the produced samples in order to study the anti-corrosion behavior of the synthesized alloys. The ASTM G102-89 was used to test the produced samples' electrochemical behavior in a 0.5 mol HCl environment at a scan rate of 0.001, with start and stop potentials of − 1.5 V and 1.5 V, respectively [20].

3 Results and Discussions

3.1 Microstructure and Composition

Figure 1 shows the SEM micrographs of Ti–Al–xNb alloys that were synthesized by varying niobium powder feedrates and the corresponding heat treatment microstructures.

It was noticed that these alloys consist of two main phase structures, the lighter phase (α-phase) and the darker phase (β-phase) characterized by dendritic microstructure in sample A3. The presence of some precipitates phase structures was also observed as depicted in Figs. 1a, e. The area of the β-phase increased with the rising content of Nb in the alloy. According to literature, the α-phase is stabilized by Al while Nb promotes stabilization of the β-phases [21–23]. Despite stabilizing important phases, the presence of these elements in the Ti–Al alloying system also induces microstructural refinement as is evident in the presented micrographs. Coarse to more fine grain

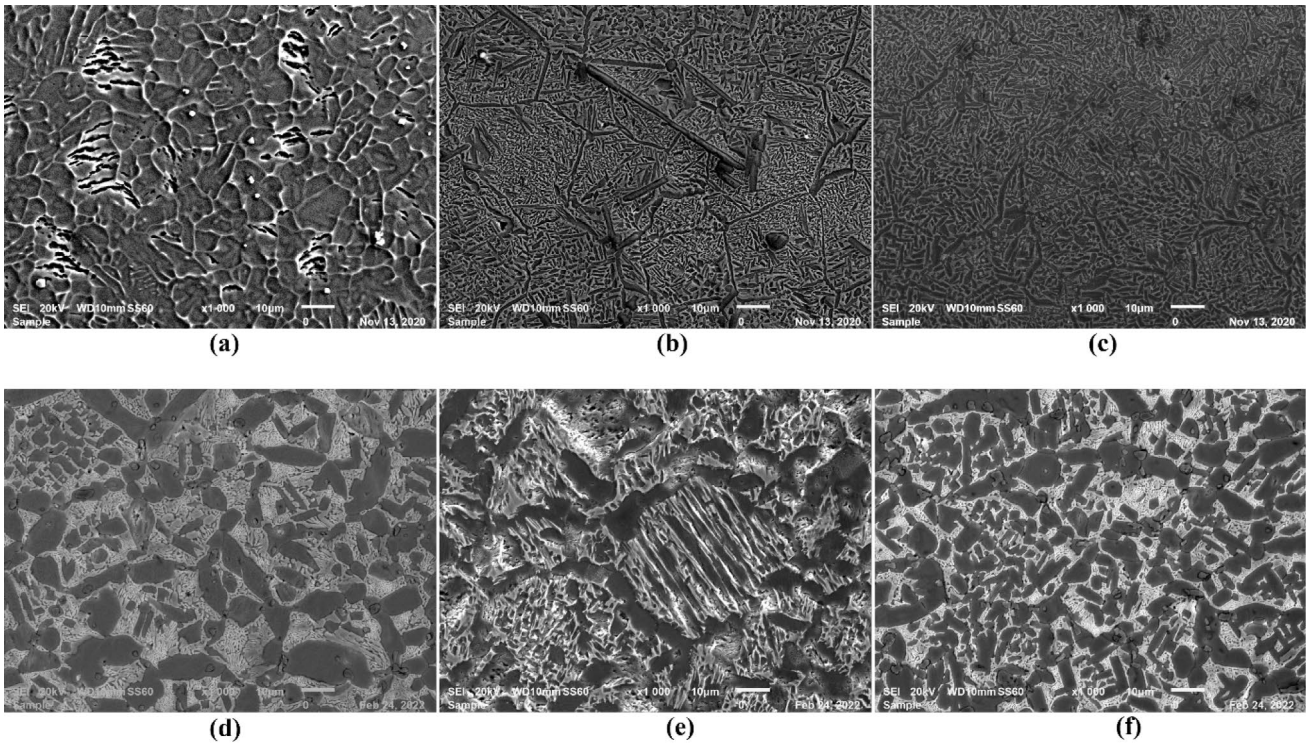

Fig. 1 The As-built TNB gamma alloys (**a**–**c**) and their corresponding heat treatment (**d**–**f**)

structures are observed in all the SEM microstructures from 0.1 rpm, 0.3 rpm to 0.5 rpm. Thus, it can be inferred that the microstructural evolution of the Ti–Al–xNb alloy is influenced by the elemental composition. Increases in the feed rate of Nb cause a gradual shift in the alloy's composition, which lowers the primary phase's volume and the solidification's temperature range, resulting in refined grain that shows no signs of cracking or stress initiation.

The EDS maps are shown in Fig. 2 also confirm the grain refinement which reveals the uniform distribution of equiaxed grains.

The equiaxed microstructure is known to contain about the same amount of α and β phases. This form of microstructure is common with important mechanical properties in the α_2-γ and β phase region. On the other hand, to achieve these microstructures, the recrystallization process can be used. Malatji and Popoola [24] posit that the alteration in grain structure observed in Nb-doped alloys indicates a decrease in thermal gradients due to the Nb's presence in the alloy matrix. The reduction of thermal gradient resulted in no cracks on the surface of the alloys. Lin and Yue [25] and Li, He [26] both stated that a low thermal gradient promotes quick nucleation, which causes fine grains to form. As a result, the morphology of the alloys transforms when Nb is added, going from an uneven shape to a fine lath shape. reaching 0.5 rpm feed rate.

The EDS map analysis as seen in Fig. 2 and summarized in Table 2 indicates the presence of a Ti–rich phase; hence the dominant dark phase in the SEM image being observed.

3.2 Dissolution of Nb

Figure 3 presents the relationship between Nb feed (at.%) and the solubility of Al (at.%) in the Ti–Al matrix.

A significant relationship that is meaningful between Nb federate and the solubility of Al could not be drawn, and indication that it might be random or more feed rate variations were needed to conclude. Nevertheless, it is with noting that the maximum dissolution of Al in the matrix was evident at 0.1 rpm while minimum solubility of Al was found at 0.3 rpm. According to Clemens [27], the enthalpy of mixing between Ti and Al was predicted to be about − 30 kJ/mol, and hence the solubility of Al to form a pure gamma phase is as anticipated when compared to − 18 kJ/mol for Al–Nb enthalpy of mixing which promotes the formation of β-Nb rich phase in the matrix.

3.3 Phase Analysis

Figure 4 present the phase analysis of the developed Ti–Al–xNb alloy.

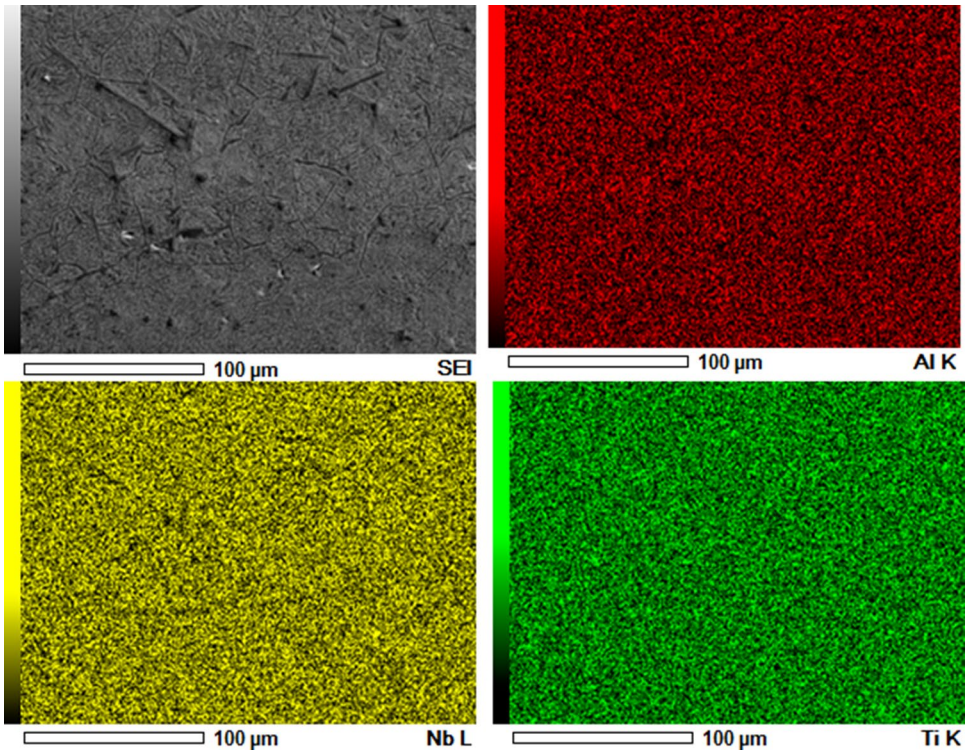

Fig. 2 EDS map of synthesized Ti–Al–xNb at 0.3 rpm Nb

Table 2 EDS summary of Ti–Al–xNb alloys

Sample ID	Ti	Al	Nb
B1	52	42	6
B3	52	36	12
B5	48	38	14

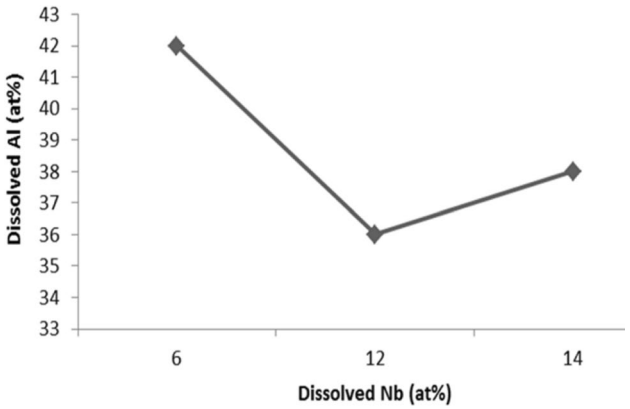

Fig. 3 Effects of niobium on aluminum solubility

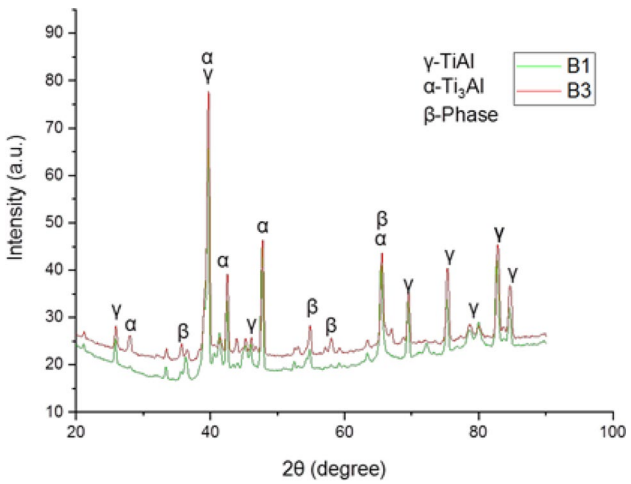

Fig. 4 XRD plots of Ti–Al–Nb alloys

The β-Nb rich phase precipitate is evident in sample B1 and sample B3 which was orthorhombic Ti_2AlNb. According to Raji, Popoola [29], the addition of Nb as a BCC β-stabilizing element incorporation to the Ti–Al alloy's matrix can enhance its RT ductility by forming minor β phase quantities. The microstructure result from Figs. 1e and 1d of the Ti–Al–xNb alloys encompasses some amount of β-rich phases along the grain boundaries with α-Ti_3Al and γ-TiAl phases. The combination of the β and γ phases is known to have moderate ductility and induce toughening, according to the study by Fischer and Laheurte [30]. In contrast, the α_2 phase imparts strengthening in the advanced γ-TiAl alloys [28].

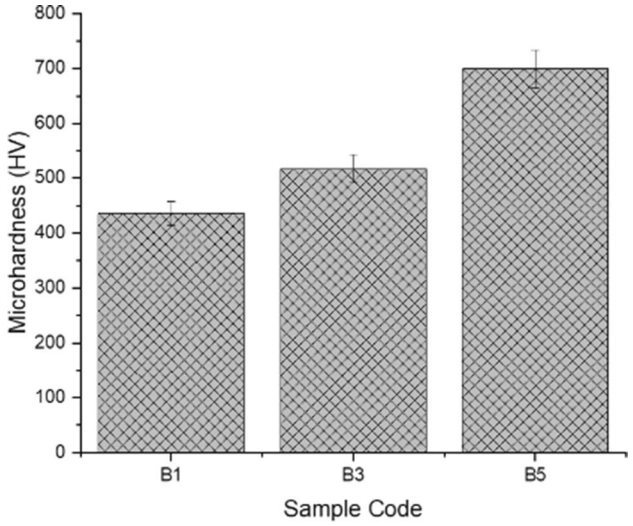

Fig. 5 Microhardness properties of the TNB alloys

3.4 Microhardness Analysis

Figure 5 shows the microhardness properties of the synthesized Ti–Al–xNb.

The mean microhardness value for TiAl–xNb with different compositions is presented in the results. Ten distinct points were used to indent the samples, and the average values are documented. With a maximum microhardness value of 697.9 HVN, sample B3 outperformed the other fabricated alloys in terms of microhardness enhancement. Sample B2 came in second with a hardness value of 518.9 HVN. The graph confirms that the increased Nb content in the alloy was the cause of the microhardness increase. In general, the quick cooling of the melt pool during laser manufacturing, which promotes the formation of small grains with excellent mechanical properties, is responsible for the strengthening mechanism of the developed TiAl–xNb alloys [31–33]. Studies in [34–36] indicate that material laser processing is also crucial for enhancing the laser-developed materials' microhardness characteristics. High microhardness, high fracture toughness, and exceptional wear resistance are among the mechanical properties that are known to be improved by the addition of Nb as an alloying element, making it useful in a variety of engineering applications.

3.5 Nano-indentation Analysis

The nano-indentation results obtained were analyzed and summarized in Table 3.

The rate of deformation under load has been an area of study for the past decades with advancements in technological devices to better understand the properties of materials and how they'll deform in different applications. The nanoindentation data presents indentation hardness (MPa), Young Modulus (GPa), and Stiffness (mN/nm) properties of the synthesized alloys. As a non-destructive method, nanoindentation has been widely used to study the microscopic mechanical response of single grains in multiphase alloys. As compared to the Ti–Al matrix, it is clear that the introduction of Nb resulted in increased indentation hardness of the developed samples with samples B3 and B5 having hardness of 77,983.0 followed by 87,606.0 MPa, respectively. The properties of hardness increased significantly for the alloy after HT. Sample B3 presented maximum hardness of 91,372.0 MPa while minimum hardness was sample B1 with hardness value of 81,657.98 MPa after normalizing HT. There was no significant variation between the stiffness and young modulus behavior of the alloys. This could be attributed to the fact that the alloy is of the same elemental composition with significant variation in composition. The ternary alloys resulted in reduced stiffness as compared to 1.145 mN/nm of the matrix. On the other hand, after HT, it is evident that the young modulus properties of the fabricated alloys drastically increased as compared to the as-built samples. The high hardness properties could be attributed to the precipitation of β-phase at the grain boundaries, resulting in a secondary phase strengthening mechanism. As a result, adding Nb improves the alloys' mechanical qualities.

3.6 Electrochemical Studies.

Figure 6 presents the polarization curves of Ti–Al–xNb in 0.5 mol of HCl.

The synthesized samples presented a high potential of more than − 0.5 V. This high potential suggests that the Ti–Al–xNb samples are more resistant to degradation in 0.5 mol of HCl as compared to commercial Ti6Al4V alloy. According to Gong et al. [3], low current density and high corrosion potential in alloys suggest that the alloy has

Table 3 Summary of nanoindentation results

Sample code	Er (GPa)	S (mN/nm)	Indentation hardness (MPa)	HT-Er (GPa)	HT-S (mN/nm)	HT-indentation hardness (MPa)
B1	153.20	0.839	74,008.8	220.12	0.71	81,657.98
B3	143.30	0.945	77,983.0	218.09	0.85	85,721.55
B5	146.08	0.856	87,606.0	222.28	0.91	91,372.01

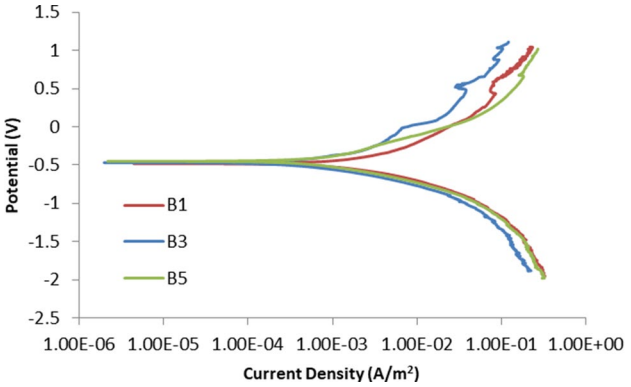

Fig. 6 Corrosion behavior of the samples

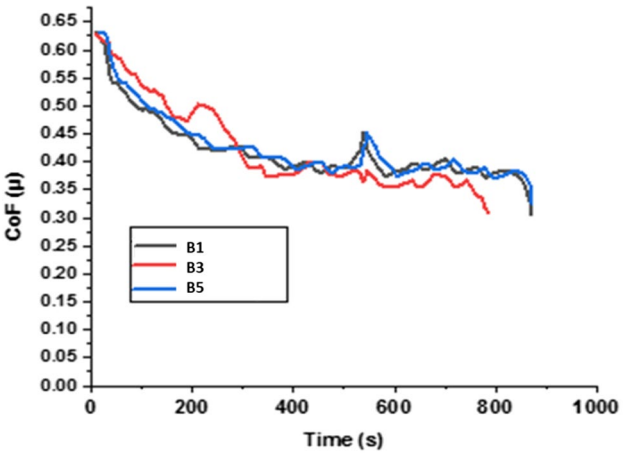

Fig. 7 CoF with time for Ti–Al–Nb alloys

Table 4 Summary of the Tafel results of Ti–Al-xNb in HCl

Sample ID	Ecorr, Obs (V)	jcorr (A/cm^2)	Corrosion rate (mm/year)	Polarization resistance (Ω)
B1	− 0.5288	1.76E-03	0.020493	6684.69
B3	− 0.5534	5.89E-03	0.068484	7116.38
B5	− 0.5125	3.11E-03	0.036140	7120.30

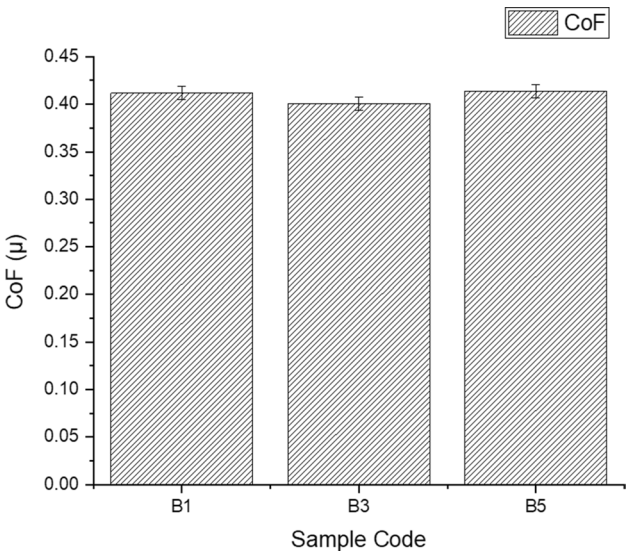

Fig. 8 Average CoF for Ti–Al–Nb alloys

superior anti-corrosive properties. Sample B5 presented high potential with a maximum value of − 0.5288 V while minimum potential value of − 0.5125 V observed in sample B5. It is noteworthy to mention that all developed samples presented oxide layer stability which prevented the samples from further corroding as it can be observed in the anodic branch reaction. Even though the potential of the material is a dependent thermodynamics variable, its role in the corrosion stability of a material cannot be neglected. The near-zero potential of all samples suggests that the developed Ti–Al–xNb samples are more resistant to corrosion. This can be attributed to the ultra-refined microstructure observed as the Nb feed rate increases. Ti–Al based alloys are known to form oxide thin film of Ti and Al along with Nb which turns to reduce the acceleration of electrochemical surface deterioration. It can be seen from the gradient of the anodic branch reaction that the alloy formed an oxide layer to decrease the rate of corrosion of the developed Ti–Al–Nb. The literature makes it clear that corrosion on the material surface may be correlated to factors such as preferential orientation, phase structure, grain size, and chemical composition. The results are summarized in Table 4.

3.7 Tribological Test

The frictional wear properties of the developed Ti–Al–xNb based alloys are presented in Fig. 7 and the average COF results are reported in Fig. 8.

It can be noted that all the Ti–Al–xNb in situ alloys gave a high CoF at the beginning of the wear test which reduced with time. Poor stability of Ti oxide film accelerates the wear rate as it easily gets damaged in contact with the stainless-steel ball. According to Adesina, Popoola [37], Ti alloys can easily wear off on the surface when they are in contact with other materials under load and in relative motion. This is as a result of the low thermal conductivity of Ti (17 W/m.k) resulting in maximum potential energy because of the high CoF at the contact position leading to initiation of stress or cracks and wear debris. The effect that Nb has on the Ti–Al matrix aids in the resistance to damage that might have accelerated the Ti–Al alloys' high frictional value. A lower CoF could be obtained by adding Nb, which could have a considerable anti-wear effect. The correlation between CoF values and Nb content was not

evident. As the Nb content increases, the mean values of the CoF were 0.412, 0.401, and 0.414 μ for sample B1, B3, and B5, respectively, as summarized by Fig. 7.

The effort and coherent precipitation of Nb to provide friction-reducing properties as a result of the refined microstructures of the in situ alloyed samples is responsible for the exceptional wear properties of the developed alloys. It's also crucial to note that the non-porous and crack-free behavior is assumed to have directly contributed to the lowest friction coefficient achieved, as the addition of Nb particles may have changed the microstructural evolution and enhanced the developed alloy.

4 Conclusion

TiAl-Nb samples were synthesized using state-of-the-art technology LENS technology. Researchers looked into how the developed Ti–Al–xNb ternary alloys' microstructural evolution, microhardness, corrosion behavior, and tribological characteristics were affected by the Nb feed rate. Microstructural evolution of the developed Ti–Al–xNb alloys showed no significant cracks or initiation of stress. It was evident from the micrographs that the increase in Nb feed rate resulted in refined microstructural evolution. The was no clear relationship between Nb dissolution in Al with process parameter (Feedrate). As the amount of Nb in the developed alloy increased, so did its microhardness properties. Maximum hardness of 697.9 HV was evident at 12at% Nb. The fabricated Ti–Al–xNb alloys demonstrated good corrosion resistance behavior in acidic environment. Minimal corrosion rate of 0.020493 mm/year was marked at sample B1 with Nb content of 4at%. Ti–Al–xNb alloys presented minimal CoF of 0.412, 0.401, and 0.414 μ for samples B1, B3, and B5, respectively.

Acknowledgements To the Council of Scientific and Industrial Research (CSIR), the National Research Foundation (NRF) and its Surface Engineering Research Laboratory (SERL), and the Department of Chemical, Metallurgical, and Materials Engineering at Tshwane University of Technology in Pretoria, South Africa, the authors would like to express their gratitude.

Author Contributions LRK contributed by doing the experimental setup and completion, writing and interpretation of the journal and experimental data, respectively; SJ contributed by assisting with data interpretation and writing review; MT contributed by interpreting the experimental data and writing review. All authors listed have significantly contributed to the development and the writing of this article.

Funding Open access funding provided by Tshwane University of Technology.

Data Availability All data used in this work are available from the corresponding author by request.

Declarations

Competing interests The authors declare no competing interests.

References

1. Huang X, Zhu L, Cai G, Liu H, Jin Z (2017) Experimental investigation of phase equilibria in the Ti–Al–Mo ternary system. J Mater Sci 52(4):2270–2284. https://doi.org/10.1007/s10853-016-0520-5
2. Tlotleng M, Lengopeng T, Seerane MN, Pityana SL (2017) Effects of heat-treatment on the microstructure of TiAl–Nb produced with laser metal deposition technique. Materials Science & Technology 2017, David L. Lawrence Convention Center, Pittsburgh, Pennsylvania, USA. http://hdl.handle.net/10204/9874
3. Gong X, Chen R, Fang H, Ding H, Guo J, Su Y, Fu H (2018) Synergistic effect of B and Y on the isothermal oxidation behavior of TiAl–Nb–Cr–V alloy. Corros Sci 131:376–385. https://doi.org/10.1016/j.corsci.2017.12.013
4. Raji SA, Popoola API, Pityana SL, Tlotleng T (2021) Microstructure and mechanical properties of heat-treated Ti–Al–Si alloy produced via laser in situ alloying. J Mater Eng Perform 30:3321–3332. https://doi.org/10.1007/s11665-021-05681-9
5. Liu HW, Bishop DP, Plucknett KP (2017) Densification behaviour and microstructural evolution of Ti–48Al consolidated by spark plasma sintering. J Mater Sci 52(1):613–627. https://doi.org/10.1007/s10853-016-0358-x
6. Liu HW, Plucknett KP (2017) Titanium aluminide (Ti–48Al) powder synthesis, size refinement and sintering. Adv Powder Technol 28(1):314–323. https://doi.org/10.1016/j.apt.2016.10.001
7. Abdulrahman KO, Akinlabi ET, Mahamood RM, Pityana S, Tlotleng M (2018) Laser metal deposition of titanium aluminide composites: a review. Mater Today: Proc 5(9):19738–19746. https://doi.org/10.1016/j.matpr.2018.06.336
8. Arthur NKK, Malabi K, Baloyi P, Moller H, Pityana SL (2016) Influence of process parameters on layer build-up and microstructure of Ti6Al4V (ELI) alloy on the optomec LENS. In: 17th Annual Conference of the Rapid Product Development Association of South Africa (RAPDASA), VUT Southern Gauteng Science and Technology Park, 2–4 November 2016. http://hdl.handle.net/10204/8992
9. Cárcel González B, Serrano A, Zambrano J, Amigó Borrás V, Cárcel González AC (2014) Laser cladding of TiAl intermetallic alloy on Ti6Al4V-process optimization and properties. Phys Procedia 56:284–293. https://doi.org/10.1016/j.phpro.2014.08.173
10. Dai J, Zhang F, Wang A, Yu H, Chen C (2017) Microstructure and properties of Ti–Al coating and Ti–Al–Si system coatings on Ti-6Al-4V fabricated by laser surface alloying. Surf Coat Technol 309:805–813. https://doi.org/10.1016/j.surfcoat.2016.10.082

11. Hirose A, Ueda T, Kobayashi KF (1993) Wear and oxidation properties of titanium aluminides formed on titanium surface by laser alloying. Mater Sci Eng A 160(1):143–153. https://doi.org/10.1016/0921-5093(93)90507-B
12. Agapovichev A, Sotov A, Kokareva V, Smelov V (2018) Possibilities and limitations of titanium alloy additive manufacturing. In: MATEC Web of Conferences, International Conference on Modern Trends in Manufacturing Technologies and Equipment (ICMTMTE 2018). EDP Sciences 224:01064 https://doi.org/10.1051/matecconf/201822401064
13. Sibisi PN, Popoola API, Arthur NKK, Pityana SL (2020) Review on direct metal laser deposition manufacturing technology for the Ti-6Al-4V alloy. Int J Adv Manuf Technol 107:1163–1178. https://doi.org/10.1007/s00170-019-04851-3
14. Cheng J, Li F, Zhu S, Yu Y, Qiao Z, Yang J (2017) Electrochemical corrosion and tribological evaluation of TiAl alloy for marine application. Tribol Int. https://doi.org/10.1016/j.triboint.2017.06.027
15. Bodunrin MO, Chown LH, van der Merwe JW, Alaneme KK (2019) Corrosion behaviour of low-cost Ti–4.5 Al–x V–y Fe alloys in sodium chloride and sulphuric acid solutions. Corros Eng Sci Technol 54(8):637–648. https://doi.org/10.1080/1478422X.2019.1654218
16. Tlotleng MP, SL, (2019) Effects of Al and heat treatment on the microstructure and hardness of Ti–Al synthesized via in situ melting using LENS. Metals 9(6):623. https://doi.org/10.3390/met9060623
17. Marashi H, Jafarlou DM, Sarhan AAD, Hamdi M (2016) State of the art in powder mixed dielectric for EDM applications. Precis Eng 46:11–33. https://doi.org/10.1016/j.precisioneng.2016.05.010
18. Zhou W, Sun X, Kikuchi K, Nomura N, Yoshimi K, Kawasaki A (2018) Carbon nanotubes as a unique agent to fabricate nanoceramic/metal composite powders for additive manufacturing. Mater Des 137:276–285. https://doi.org/10.1016/j.matdes.2017.10.034
19. Izadi M, Farzaneh A, Mohammed M, Gibson I, Rolfe B (2020) A review of laser engineered net shaping (LENS) build and process parameters of metallic parts. Rapid Prototyp J 26:1059–1078. https://doi.org/10.1108/RPJ-04-2018-0088
20. ASTM, G (2004) Standard practice for calculation of corrosion rates and related information from electrochemical measurements. G102–89.
21. Srivastava D, Chang I, Loretto M (2001) The effect of process parameters and heat treatment on the microstructure of direct laser fabricated TiAl alloy samples. Intermetallics 9(12):1003–1013. https://doi.org/10.1016/S0966-9795(01)00063-2
22. Ma S, Zhang Y (2012) Effect of Nb addition on the microstructure and properties of AlCoCrFeNi high-entropy alloy. Mater Sci Eng A 532:480–486. https://doi.org/10.1016/j.msea.2011.10.110
23. Riveiro A, Mejías A, Lusquiños F, del Val J, Comesaña R, Pardo J, Pou J (2013) Optimization of laser cladding for Al coating production. Phys Procedia 41:327–334. https://doi.org/10.1016/j.phpro.2013.03.085
24. Malatji N, Popoola API, Lengopeng T, Pityana SL (2020) Effect of Nb addition on the microstructural, mechanical and electrochemical characteristics of AlCrFeNiCu high-entropy alloy. Int J Miner Metall Mater 27(10):1332–1340. https://doi.org/10.1007/s12613-020-2178-x
25. X, Yue TM, (2005) Phase formation and microstructure evolution in laser rapid forming of graded SS316L/Rene88DT alloy. Mater Sci Eng A 402(1–2):294–306. https://doi.org/10.1016/j.msea.2005.05.024
26. Li MX, He YZ, Sun GX (2005) Microstructure of ODS superalloy coating produced by laser surface cladding. Rare Metal Mater Eng 34(2):248–251
27. Clemens H, Bartels A, Bystrzanowski S, Chladil H, Leitner H, Dehm G, Gerling R, Schimansky FP (2006) Grain refinement in γ-TiAl-based alloys by solid state phase transformations. Intermetallics 14(12):1380–1385. https://doi.org/10.1016/j.intermet.2005.11.015
28. Liu J, Dahmen M, Ventzke V, Kashaev N, Poprawe R (2013) The effect of heat treatment on crack control and grain refinement in laser beam welded β-solidifying TiAl-based alloy. Intermetallics 40:65–70. https://doi.org/10.1016/j.intermet.2013.04.007
29. Raji SA, Popoola API, Pityana SL, Popoola OM (2020) Characteristic effects of alloying elements on β solidifying titanium aluminides: a review. Heliyon 6(7):e04463. https://doi.org/10.1016/j.heliyon.2020.e04463
30. Fischer FD, Waitz T, Scheu C, Cha L, Dehm G, Antretter T, Clemens H (2010) Study of nanometer-scaled lamellar microstructure in a Ti–45Al–7.5 Nb alloy—experiments and modeling. Intermetallics 18(4):509–517. https://doi.org/10.1016/j.intermet.2009.09.012
31. Masina BN, Skhosane S, Hoosain S, Tlotleng M (2020) Effect of in-situ heat treatment and process parameters on the laser-deposited IN718 microstructure and mechanical properties. MRS Adv 5(23):1245–1257. https://doi.org/10.1557/adv.2020.213
32. Iijima D, Yoneyama T, Doi H, Hamanaka H, Kurosaki N (2003) Wear properties of Ti and Ti–6Al–7Nb castings for dental prostheses. Biomaterials 24(8):1519–1524. https://doi.org/10.1016/S0142-9612(02)00533-1
33. Distl B, Dehm G, Stein F (2020) Effect of oxygen on high-temperature phase equilibria in ternary Ti–Al–Nb alloys. Z Anorg Allg Chem 646:1151–1156. https://doi.org/10.1002/zaac.202000098
34. Lazurenko DV, Laptev IS, Golkovsky MG, Stark A, Paul J, Bataev I, Ruktuev AA, Gollwitzer SL, C, Pyczak F, (2020) Influence of the Ti/Al/Nb ratio on the structure and properties on intermetallic layers obtained on titanium by non-vacuum electron beam cladding. Mater Charact 163:110246. https://doi.org/10.1016/j.matchar.2020.110246
35. Ng C, Bermingham M, Kent D, Dargusch M (2021) High stability and high strength β-titanium alloys for additive manufacturing. Mater Sci Eng, A 816:141326. https://doi.org/10.1016/j.msea.2021.141326
36. Raji SA, Popoola API, Pityana SL, Popoola OM, Arthur NKK, Tlotleng M (2021) Influence of Mo on microstructure and nanoindentation hardness of Ti–Al–Si–xMo alloy processed by laser engineered net shaping (LENS). Suid-Afrikaans Tydskrif vir Natuurwetenskap en Tegnologie/South African Journal of Science and Technology, 40(1):91–97. https://hdl.handle.net/10520/ejc-aknat_v40_n1_a34
37. Adesina OS, Popoola API, Pityana SL, Oloruntoba DT (2018) Microstructural and tribological behavior of in situ synthesized Ti/Co coatings on Ti-6Al-4V alloy using laser surface cladding technique. Int J Adv Manuf Technol 95(1–4):1265–1280. https://doi.org/10.1007/s00170-017-1300-3